


Superfluidity of indirect excitons in van der Waals heterostructures of transition metal trichalcogenides

Roman Ya. Kezerashvili  and Anastasia Spiridonova 

*Physics Department, New York City College of Technology, The City University of New York, Brooklyn, New York 11201, USA
and The Graduate School and University Center, The City University of New York, New York, New York 10016, USA*

 (Received 22 August 2022; revised 8 November 2022; accepted 12 December 2022; published 23 December 2022)

We predict angle-dependent superfluidity for a new class of two-dimensional materials: transition metal trichalcogenides (TMTC). Within a mean-field approach superfluidity of indirect excitons in TMTC van der Waals heterostructures (vdWHs) is studied. We use different potentials for charged carrier interaction to analyze the influence of the screening on the studied phenomena. Our study demonstrates the angle-dependent superfluidity temperature in TMTC vdWHs: for a given density a maximum and minimum T_c of superfluidity occurs along the chain and a directions, respectively. This work can guide experimental research toward the realization of anisotropic superfluidity in TMTC vdWH. We suggest an experiment for the observation of anisotropic superfluidity in TMTC vdWH.

DOI: [10.1103/PhysRevB.106.245306](https://doi.org/10.1103/PhysRevB.106.245306)

I. INTRODUCTION

Pairing of electrons and holes bound by the electrostatic attraction in a system consisting of two spatially separated electron and holes layers was proposed as a possible origin of superfluidity initially in coupled semiconductor quantum wells [1]. Following this, a very substantial fraction of theoretical and experimental works have been devoted to the study of Bose-Einstein condensation (BEC) and superfluidity of indirect interlayer excitons (see reviews [2,3]). After the discovery of graphene, electron-hole superfluidity has been studied in a different new class of two-dimensional (2D) materials [4–16]. On one hand, gapped graphene, Xenes, and transition metal trichalcogenides (TMDCs) are 2D materials with isotropic carrier particle masses, where superfluidity of a dipolar Bose gas is isotropic [4–8,10–12,14,15]. On the other hand, phosphorene, group-V TMDCs (ReS₂ and ReSe₂), and TMTCs have asymmetric electron-hole masses along the x and y directions [17–20]. We cite these works, but the recent literature on the subject is not limited by them.

The anisotropic superfluidity for quasiparticles was first studied for He³ [21]. The superfluid character of a dipolar BEC in a quasi-two-dimensional geometry and anisotropic superfluidity in a superfluid system with anisotropic effective masses along principal three-dimensional (3D) directions were investigated in Refs. [17,20]. There has been a particular interest in the study of superfluidity of indirect excitons in anisotropic van der Waals heterostructures (vdWH) with phosphorene sheets separated by thin hBN insulating layers. It was predicted in Ref. [18] the angular dependence of the mean-field critical temperature for superfluidity in a weakly interacting gas of dipolar excitons in phosphorene vdWH. The anisotropic superfluidity is predicted in Ref. [19], where it was found that the maximum superfluid gap in the BEC

regime is along the armchair direction. While a special feature of phosphorene is the high in-plane anisotropy of its energy band structure that leads to dipole exciton anisotropic superfluidity, phosphorene is unstable in air and highly toxic.

A stream of new 2D layered materials has been developed over the past 10 years. Among them, there exist a small number of materials with strong in-plane structural anisotropy such as transition metal trichalcogenides (TMTCs): TiS₃, TiSe₃, ZrS₃, and ZrSe₃. In contrast to TiS₃, TiSe₃, ZrS₃, and ZrSe₃ monolayers are all indirect gap semiconductors [22,23]. There are several reasons to seriously consider the TMTC family: they are environmentally friendly, have low manufacturing cost of semiconductors, and forbid native oxide formation. These motivate us to study superfluidity in TMTC.

Heterostructures with two parallel TMTC monolayers with one n -doped and the other p -doped, respectively, separated by an insulating barrier of stacked hBN monolayers to block electron-hole recombination [24] is an interesting platform for investigation of electron-hole superfluidity. It is assumed that 2D layers are populated with carriers of opposite polarity and equal density. In such kind of platform due to electrostatic interaction electrons and holes can pair to produce dipole (indirect) excitons, which are composite bosons [25]. This kind of the system was used to study the effect of superfluidity in heterostructures composed with graphene, TMDC, and phosphorene monolayers [8,9,11,12,18,19].

In this paper, we predict superfluidity of indirect excitons in van der Waals heterostructures composed of TMTC monolayers and demonstrate that the mean-field critical temperature is angle dependent: for a given density a maximum temperature of superfluidity occurs along chain direction while a minimum temperature occurs along the a direction. In addition, we propose an experiment for observation of this phenomenon in TMTC heterostructure.

II. MODEL, RESULTS, AND DISCUSSIONS

To explore a feasibility of superfluidity of paired spatially separated electrons and holes first consider the formation of indirect excitons (IXs), in TMTC heterostructure. In the framework of the effective mass approximation, after the separation of the center of mass, the Schrödinger equation for the relative motion of an interacting electron-hole pair with anisotropic masses in TMTC vdWH reads as $[-\frac{1}{2\mu_x}\frac{\partial^2}{\partial x^2} - \frac{1}{2\mu_y}\frac{\partial^2}{\partial y^2} + V(x, y)]\Phi(x, y) = E\Phi(x, y)$, where $\mu_x = \frac{m_x^e m_x^h}{m_x^e + m_x^h}$ and $\mu_y = \frac{m_y^e m_y^h}{m_y^e + m_y^h}$ are the anisotropic reduced masses in the x and y directions, respectively, m_x^e (m_x^h) and m_y^e (m_y^h) correspond to the electron (hole) effective masses along the x and y directions, and $\Phi(x, y)$ is the electron-hole pair relative motion wave function. However, for now note that, according to [26–29], the a direction ($\theta = 0$) corresponds to the x direction, and the b direction ($\theta = \pi/2$) corresponds to the y direction.

The interaction potential $V(x, y)$ between the electron and hole which resides in two different TMTC monolayers is $V_C(x, y) = -\frac{ke^2}{\kappa(\sqrt{x^2+y^2+D^2})}$ in the case of the Coulomb electrostatic attraction or

$$V_{\text{RK}}(x, y) = -\frac{\pi ke^2}{2\kappa\rho_0} \left[H_0 \left(\frac{\sqrt{x^2+y^2+D^2}}{\rho_0} \right) - Y_0 \left(\frac{\sqrt{x^2+y^2+D^2}}{\rho_0} \right) \right] \quad (1)$$

if the indirect exciton is formed via the Rytova-Keldysh (RK) potential [30,31]. These two equations describe the interaction between the electron and hole that is located in two parallel TMTC monolayers separated by a distance $D = h + Nl_{\text{hBN}}$, where $l_{\text{hBN}} = 0.333$ nm is the thickness of the hBN layer, N is the number of hBN layers, and h is the TMTC monolayer thickness. In Eq. (1) e is the charge of the electron, $\kappa = (\epsilon_1 + \epsilon_2)/2$ describes the surrounding dielectric environment, ϵ_1 and ϵ_2 are the dielectric constants below and above the monolayer, respectively, H_0 and Y_0 are the Struve and Bessel functions of the second kind, respectively, and ρ_0 is the screening length. The potential (1) has the same functional form as the one derived in Ref. [32], where the macroscopic screening is quantified by the 2D polarizability. Following [32,33] the screening length ρ_0 can be written as $\rho_0 = 2\pi\chi_{2\text{D}}/\kappa$, where $\chi_{2\text{D}}$ is the 2D polarizability. 2D layer polarizability can be computed by standard first-principles technique [32] or considered as a phenomenological parameter. Below for indirect excitons, we report calculations for both the Coulomb and RK (1) potentials to explore the role of the screening.

Our goal is to engineer vdWH with a high-exciton binding energy. By averaging the Schrödinger equation, one can obtain the expectation value for the bound-state energies: $E = \langle -\frac{1}{2\mu_x}\frac{\partial^2}{\partial x^2} \rangle + \langle -\frac{1}{2\mu_y}\frac{\partial^2}{\partial y^2} \rangle + \langle V(x, y) \rangle$. The terms in this expression could be viewed as the sum of the average values of the operators of kinetic and potential energies in 2D space obtained by using the corresponding eigenfunction $\Phi(x, y)$. From this expression it follows that large reduced masses μ_x and μ_y give small contributions of the kinetic energy terms

that lead to larger binding energy. We examined vdWHs composed of two the same and two different TMTC monolayers. Based on our results for binding energies of IXs, we have selected the following heterostructures where excitons have the largest binding energies: ZrSe₃/ZrS₃, TiS₃/ZrS₃, TiS₃/ZrSe₃, ZrS₃/ZrS₃, ZrSe₃/ZrSe₃. The charge carrier in the first layer is electrons and in the second one is holes. The binding energies of excitons increase from about 73 to 89 meV for the RK potential and from about 105 to 133 meV for the Coulomb potential when TMTC monolayers are separated by a single hBN layer. The increase of the hBN layers reduces the binding energies of excitons monotonically. For six hBN layers the energies vary from 49 to 57 meV for the RK potential and from 58 to 68 meV for the Coulomb potential. Thus, the difference between exciton binding energies obtained with the Coulomb and RK potentials decreases. The binding energies of indirect excitons in vdWHs are given in Table I in Appendix A. Thus, we can conclude that a dilute gas of bound excitons can be induced in TMTC vdWHs.

We now turn our attention to a dilute gas of bound electrons and holes in TMTC vdWHs, when $nr_X^2 \ll 1$, where n and r_X are the concentration and radius for indirect excitons, respectively. Under this condition, we treat the dilute system of indirect excitons in TMTC vdWH as a weakly interacting Bose gas.

The excitons are composite bosons [25] and at large interlayer separations, the exchange effects [2,34] in the exciton-exciton interactions in a TMTC vdWHs can be neglected since the exchange interactions in vdWH are suppressed due to the low tunneling probability, caused by the shielding of the dipole-dipole interaction by the insulating barrier. When an electron and hole are located in two different monolayers, the electron-hole forms an energetically favorable configuration where dipoles are parallel to each other.

Consider excitons as composite bosons [25] forming a weakly interacting Bose gas of direct excitons in TMTC vdWH. A general form of a many-body Hamiltonian for the 2D interacting IXs in second quantization reads as [35,36]

$$\hat{H} = \sum \varepsilon_0(p, \theta) a_{\mathbf{p}}^\dagger a_{\mathbf{p}} + \frac{g}{S} \sum a_{\mathbf{p}_1}^\dagger a_{\mathbf{p}_2}^\dagger a_{\mathbf{p}_1} a_{\mathbf{p}_2}, \quad (2)$$

where summation of all impulses appearing in indices, $a_{\mathbf{p}}^\dagger$ and $a_{\mathbf{p}}$ are Bose creation and annihilation operators for IXs with momentum \mathbf{p} , S is a normalization area for the system, g is a coupling constant for the interaction between two IXs, and $\varepsilon_0(p, \theta)$ is the angle-dependent energy spectrum of noninteracting indirect excitons $\varepsilon_0(\mathbf{p}) = \frac{p_x^2}{2M_x} + \frac{p_y^2}{2M_y} = \frac{p^2}{2M_0(\theta)}$, where $p_x = p \cos \theta$ and $p_y = p \sin \theta$ are the polar coordinates for the center-of-mass momentum \mathbf{p} and $M_0(\theta) = [\frac{\cos^2 \theta}{M_x} + \frac{\sin^2 \theta}{M_y}]^{-1}$ is the angle-dependent effective mass, where $M_x = (m_x^e + m_x^h)$ and $M_y = (m_y^e + m_y^h)$. The only difference between (2) and the Hamiltonian for isotropic excitons of weakly interacting Bose gas is that the single-particle energy spectrum of noninteracting excitons is angle dependent due to the angular dependence of the exciton effective mass $M_0(\theta)$.

Consider a weakly interacting gas of IXs in a TMTC heterostructure in the framework of the Bogoliubov approximation. The chemical potential of the interacting dilute Bose

gas is given by $\mu = gn$ [35–37] and following the standard textbook procedure [36], one obtains

$$\hat{H} = E_0 + \sum_{\mathbf{p} \neq 0} \epsilon(p, \theta) b_{\mathbf{p}}^{\dagger} b_{\mathbf{p}}, \quad (3)$$

where E_0 is the ground-state energy [36], $b_{\mathbf{p}}^{\dagger}$ and $b_{\mathbf{p}}$ are the new set of creation and annihilation Bose operators for the quasiparticles that follow the same Bose commutation relations $b_{\mathbf{p}} b_{\mathbf{p}'}^{\dagger} - b_{\mathbf{p}'}^{\dagger} b_{\mathbf{p}} = \delta_{\mathbf{p}\mathbf{p}'}$ obeyed by the original particle operators $a_{\mathbf{p}}^{\dagger}$ and $a_{\mathbf{p}}$, and

$$\begin{aligned} \epsilon(p, \theta) &= \left[\frac{gn}{M_0(\theta)} p^2 + \left(\frac{p^2}{2M_0(\theta)} \right)^2 \right]^{1/2} \\ &= [\epsilon_0(p, \theta) + \mu]^2 - \mu^2]^{1/2} \end{aligned} \quad (4)$$

is the famous Bogoliubov dispersion law for the elementary excitations of the system obtained in 1947 [38]. In our case, due to the mass anisotropy, the spectrum of collective excitations $\epsilon_0(p, \theta)$ depends on the angle θ , while the exciton-exciton interaction term is angle independent. Thus, the angle-dependent spectrum of the collective excitations $\epsilon(p, \theta)$ turns out to be uniquely fixed by the interaction between two dipolar excitons, i.e., by the coupling constant g . The derivation of the coupling constant g is given in Appendix B.

Introduce the mean-field critical temperature $T_c(\theta)$. At nonzero temperatures, the density of the superfluid component $\rho_s(T)$ is defined as $\rho_s(T) = \rho - \rho_n(T)$, where ρ is the total 2D density of the exciton gas and $\rho_n(T)$ is the density of the normal component [39]. Suppose that the excitonic system moves with a velocity \mathbf{u} , which means that the superfluid component moves with the velocity \mathbf{u} . To calculate the density of the superfluid component consider the total density flow \mathbf{J} [40] for a Bose gas of quasiparticles. Following Ref. [21] and restricting oneself to the first-order term, in the reference frame where the superfluid component is at rest, one obtains $\mathbf{J} = -\frac{s}{k_B T} \int \frac{d^2 p}{(2\pi \hbar)^2} \mathbf{p}(\mathbf{p}\mathbf{u}) \frac{\partial f[\epsilon(p, \theta)]}{\partial \epsilon(p, \theta)}$. In the latter expression $f[\epsilon(p, \theta)] = (\exp[\epsilon(p, \theta)/(k_B T)] - 1)^{-1}$ is the Bose-Einstein distribution function for quasiparticles with anisotropic quasiparticle energy $\epsilon(p, \theta)$, $s = 4$ is the spin degeneracy factor, and k_B is the Boltzmann constant. The normal density ρ_n for the anisotropic system has a tensor form [21] and is defined through the component of density flow \mathbf{J} vector as $J_i = \rho_n^{ij}(T) u_j = \frac{n_n^{ij}(T)}{M_j} u_j$, where i and j denote either the x or y components of the vector, and $n_n^{(ij)}(T)$ are the tensor elements of normal concentration. In a superfluid with an anisotropic quasiparticle energy, the normal-fluid concentration is a diagonal tensor [21] such that $n_n^{xy}(T) = n_n^{yx}(T) = 0$, and expressions for n_n^{xx} and n_n^{yy} are given in Appendix C. At last, the concentration of the normal component is

$$n_n(\theta, T) = \sqrt{n_n^{xx}(T)^2 \cos^2 \theta + n_n^{yy}(T)^2 \sin^2 \theta}. \quad (5)$$

Finally, the mean-field critical temperature $T_c(\theta)$ of the phase transition related to the occurrence of superfluidity is determined by the condition $n_n(\theta, T_c(\theta)) = n$, where n is a total exciton concentration.

Our main results are summarized in the contour plots presented in Figs. 1(a)–1(c), where we report T_c for superfluidity with the spectrum of collective excitations given by Eq. (4). The results for soundlike spectrum are given in Appendix D. While examining T_c obtained with the Bogoliubov energy spectrum (4) and the soundlike spectrum (Appendix C), we have found that vdWH that are composed of the same TMTC monolayers have higher T_c than vdWHs composed from two different TMTC monolayers.

In calculations, we consider the excitonic concentrations in the range of 6×10^{15} to $3 \times 10^{16} \text{ m}^{-2}$. The indirect exciton concentrations $n \sim 6 \times 10^{15} \text{ m}^{-2}$ are achievable in 2D TMDC heterostructures. For instance, the estimated IXs concentration for the optimal indirect excitons propagation condition in Ref. [41] is $n \sim 6 \times 10^{15} \text{ m}^{-2}$. The concentrations $\sim 2\text{--}3 \times 10^{16} \text{ m}^{-2}$ can be achieved for indirect excitons in 2D TMDC heterostructures, and order of $1\text{--}8 \times 10^{16} \text{ m}^{-2}$ in single-layer black phosphorus [42]. However, one should mention that high densities approach the Mott transition [8], beyond which the hydrogenlike indirect excitons vanish and the Cooper-pair-like excitons may form. The latter were observed in the GaAs heterostructure [43]. In Fig. 1(a) results of calculations for T_c using the Coulomb and RK potentials are presented for ZrS₃ and TiS₃ vdWHs. T_c obtained using the Coulomb potential is more than twice as big as one calculated with the RK potential. This difference is due to the strong screening of the RK potential. Interestingly enough, the ratios of T_c along the chain direction (b axis) to T_c along the a axis do not depend on the potential and are 1.07 and 1.33 for TiS₃ and ZrS₃ vdWH, respectively. Thus, ZrS₃ demonstrates a stronger angle dependent T_c . It is interesting to compare T_c for ZrS₃ and phosphorene. For example, in the case of phosphorene T_c at the concentration $3 \times 10^{16} \text{ m}^{-2}$ has maximum at $\theta = 0$ and minimum when $\theta = \pi/2$ [18], in contrast to ZrS₃ where T_c has minimum at $\theta = 0$ and maximum at $\theta = \pi/2$.

In Fig. 1(b) results of calculations are presented for ZrS₃ vdWH for different concentrations of exciton gas and one data set for TiS₃ vdWH when $n = 2 \times 10^{16} \text{ m}^{-2}$. From the polar plot, it can clearly be seen that for ZrS₃ the critical temperature of superfluidity is aligned along the chain direction (b axis) for all considered excitonic concentrations. T_c increases as the concentration increases. The maximum T_c is observed along the chain direction at $\theta = \pi/2$, while minimum T_c is observed along the a axis ($\theta = 0$). An interesting observation is that the ratio $T_{c \text{ max}}/T_{c \text{ min}}$ almost does not depend on the excitonic concentration and decreases monotonically from 1.34 at $n = 6 \times 10^{15} \text{ m}^{-2}$ to 1.33 at $n = 3 \times 10^{16} \text{ m}^{-2}$. The behavior of T_c for TiS₃ appears almost isotropic with $T_{c \text{ max}}/T_{c \text{ min}} = 1.07$. This phenomenon can be explained by the fact that μ_x and μ_y are almost equal to each other (very small mass anisotropy along x and y). In addition, as can be seen in Fig. 1(c), the increase in the number of insulating hBN layers N leads to the increase of T_c .

As stated above, our studies reveal that the maximum T_c occurs along the chain direction. This can be explained by TMTC monolayer structure. The simplest description of geometrical structures known as quasi-one-dimensional compounds is usually in terms of the condensation of small clusters of atoms into infinite chains. In TMTCs, trigonal

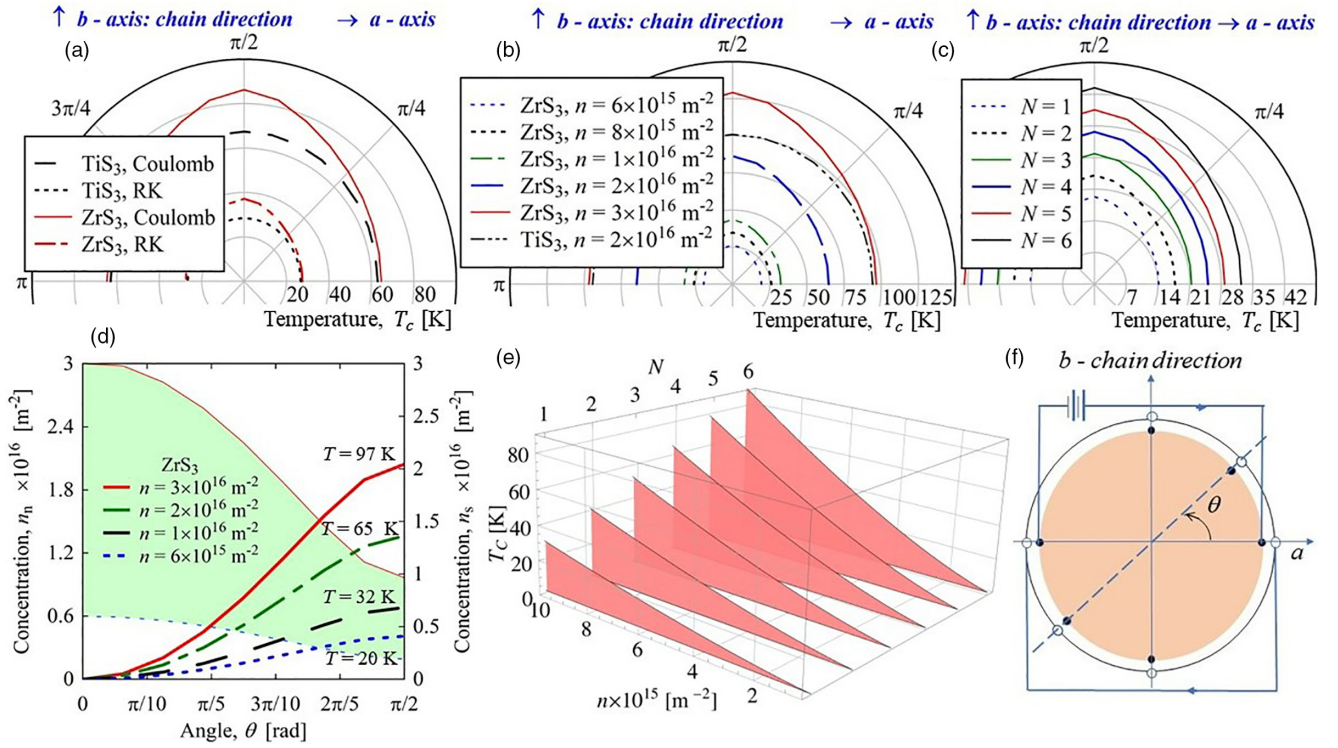


FIG. 1. The contour plot for the angle-dependent mean-field critical temperature for superfluidity T_c in polar coordinates for IXs (a) when $n = 3 \times 10^{16}$ and $8 \times 10^{15} \text{ m}^{-2}$ in ZrS_3 vdWH (solid and dotted-dashed curves, respectively) and TiS_3 vdWH (dashed and dotted curves, respectively) using the Coulomb and RK potentials and $N = 6$; (b) T_c at different excitonic concentrations in ZrS_3 vdWH. The calculation for TiS_3 vdWH is performed at $n = 2 \times 10^{16} \text{ m}^{-2}$ using the Coulomb potential and $N = 6$. (c) T_c for different numbers of hBN layers when $n = 1 \times 10^{16} \text{ m}^{-2}$. The calculations are performed using the Coulomb potential. (d) Thick curves show the angle dependence of the superfluid concentration for different total concentrations of the excitonic gas at the corresponding T_c at which the superfluidity vanishes along the a axis. Two thin curves bound green shaded region that shows the angle dependence of the normal concentration. (e) T_c for indirect excitons in TiS_3 vdWHs in the limit of the sound-like spectrum of collective excitations as a function of concentration and interlayer separation. The calculations are performed for the Coulomb potential. (f) A schematic plan view for a suggested experiment. The “active” and parallel “passive” layers are shown as shaded and white areas, respectively. Filled and open dots indicate contacts to the “active” and “passive” layers, respectively.

prismatic units MX_6 with six atoms of chalcogenides and one atom of transition metal condense laterally into the two-dimensional layers of MX_3 and longitudinally into the one-dimensional linear chains of the MX_6 . In other words, these compounds crystallize in a chain structure [44] composed of wedge-shaped trigonal prisms stacked one on top of the other, base to base, while the metal atom at the center of each prism is coordinated to six chalcogen atoms at the corners of the prisms.

For instance, ZrS_3 has a rather strong in-plane structural anisotropy due to weak chain-chain interaction. Each ZrS_3 layer consists of 1D chains made of MX_6 octahedrons extending along the b direction [22,45,46] that are weakly coupled laterally in the a -axis direction where the M - X linkages between chains via two chalcogen atoms in neighboring chains are held together weakly by forces of the van der Waals type. Inside the 1D prismatic chain, the unit orientated along b , six atoms of S are equally separated from the metal atom Zr at $\sim 2.63 \text{ \AA}$, but the S atoms outside of the chain are slightly farther away $\sim 2.75 \text{ \AA}$ [46]. This difference in bonds' length results in slightly decoupled 1D-chain-like structures confined in the ab plane. It is worth noting the results for bonds' length stated above are consistent with earlier structural studies on ZrS_3 [22,47,48]. The conclusion drawn from the study [47]

was that the strength of the coupling between the chains was approximately $\frac{1}{5}$ of the strength of the M - X bond within the chain. Thus, our results indicate that the maximum T_c occurs along the quasi-one-dimensional linear chains of the ZrS_3 .

In Fig. 1(d) using thick lines, we show the dependence of the superfluid concentration n_s on the angle for different total concentrations n of the dipole excitons at temperatures at which the superfluidity is killed. In other words, we take T_c at which superfluidity is killed when $\theta = 0$ (a axis), then we keep T_c constant and increase θ and calculate n_s . The concentration of the superfluid component increases with the increase of θ and achieves the maximum at $\theta = \pi/2$, which corresponds to chain direction. In addition, we show the angular dependence of the normal concentration n_n that falls within a green shaded area between the thin red solid and dashed blue curves obtained for $n = 3 \times 10^{16} \text{ m}^{-2}$ at $T_c = 97 \text{ K}$ and $n = 6 \times 10^{15} \text{ m}^{-2}$ at $T_c = 20 \text{ K}$, respectively.

In our calculations with RK potential, we use the isotropic approximation for the 2D polarizability. In general, 2D polarizability of anisotropic materials should be considered as a tensor. However, following Ref. [49], we used rather crude approximation $\chi_{2D,xx} = \chi_{2D,yy}$, and replaced both by their average. In Refs. [27,50,51] the isotropic approximation of 2D polarizability was also used. This approximation simplifies the

calculation in case of RK potential and did not affect substantially exciton binding energy [49], in contrast to electron-hole mass anisotropy.

In the limit of small momenta p , when $\varepsilon_0(p, \theta) \ll gn$, we expand the spectrum of collective excitations $\varepsilon(p, \theta)$ up to first order with respect to the momentum p and obtain the sound mode of the collective excitations $\varepsilon(p, \theta) = c_s(\theta)P$, where $c_s(\theta)$ is the angle-dependent sound velocity given in Appendix D. Since at low momenta the soundlike energy spectrum of collective excitations of the IXs in a TMTC heterostructure satisfies the Landau criterion for superfluidity, the superfluidity of IXs in this system is possible. Thus, such systems below the Berezinskii-Kosterlitz-Thouless (BKT) transition temperature may support a superflow of indirect excitons. One can estimate the BKT phase transition temperature from the condition $n_n(T) = n$. The latter leads to

$$T_{\text{BKT}} = \left(\frac{\pi(\hbar g)^2}{2\zeta(3)s\sqrt{M_x M_y}} \right)^{1/3} \frac{n}{k_B} \quad (6)$$

and can be considered as an upper bound to the superfluid transition temperature.

Exclusivity of TiS_3 monolayer which has a direct band gap motivates us to calculate T_c for TiS_3 vdWH in the limit for the soundlike spectrum of collective excitations. The T_c for IXs in TiS_3 vdWH as a function of concentration and number of hBN insulating layers is shown Fig. 1(e). Calculations are performed with the Coulomb potential. T_c increases with the increase of the concentration and interlayer separation.

The angle-dependent superfluidity in TMTC vdWHs may be observed in electron-hole Coulomb drag experiments [52]. In such experiment, a voltage is applied to the one of the layers, known as the ‘‘active’’ layer. The other ‘‘passive’’ layer is closed upon itself by connecting to an external resistor. The electric current in the active layer induces a current in the passive layer in the opposite direction by means of the Coulomb drag, i.e., by the momentum transfer due to the interlayer electron-hole interaction. The drag current is typically much smaller than the drive current owing to the heavy screening of the Coulomb interaction [53].

A schematic plan view for the suggested experiment is shown in Fig. 1(f). The geometry of the experiment revealing the existence of the exciton angle-dependent superfluidity will include measurements at the angle $\theta = 0$ with respect to the a axis at the corresponding transition temperature T_c for the given excitonic concentration n when there is no superfluidity. At the next step, one applies voltage to active layer at the angle θ and makes measurement in the passive layer at the same angle. By keeping T_c constant and gradually increasing the angle θ with respect to the a axis and making measurements of the induced current in the passive layer, let us say at $\theta = \pi/6$, $\theta = \pi/4$, $\theta = \pi/3$, and $\theta = \pi/2$ (at the same angles the voltage is applied to the active layer), one can observe the increment of the induced current with the increase of θ . The maximum value is achieved in the chain direction at $\theta = \pi/2$. In such measurements, due to the electron-hole mass anisotropy, there is no induced current at T_c , which corresponds to the a axis direction, and there is the maximal current at this temperature in the chain direction. If instead of the superfluid current, the normal current is measured at T_c when n_c has the minimum

based on results in Fig. 1(f) one will observe the opposite picture: the normal current depletion from the maximum at $\theta = \pi/2$ to the minimum at $\theta = 0$. While the purely Coulomb drag can be the most qualitative features of the effect, other mechanisms of momentum transfer can also contribute to the observed behavior [52].

III. CONCLUSIONS

To conclude, in the framework of a mean-field approach within the Bogoliubov approximation, we predict angle-dependent superfluidity of indirect excitons in van der Waals heterostructures composed from a new class of two-dimensional materials: TMTC. The angle-dependent superfluidity is due to the directional anisotropy of the electron and hole effective masses. The angle dependence of T_c occurs beyond the soundlike approximation for the spectrum of collective excitation: for a given density a maximum and minimum T_c of superfluidity is along the chain and a directions, respectively. Thus, in contrast to the anisotropic behavior of T_c for phosphorene [18], the vastly different angular dependence of T_c is observed for ZrS_3 . In calculations, we used the Rytova-Keldysh and Coulomb potentials for charged carrier interaction to analyze the influence of the screening. For both potentials the angle-dependent superfluidity of indirect excitons is observed. The critical temperature for the phase transition obtained using the Coulomb potential is significantly larger than T_c calculated with the RK potential. Thus, our results demonstrate that the screening does significant affect the phase transition temperature. We have reported binding energies for indirect excitons in vdWH composed of two different and the same TMTC monolayers. The indirect excitons bound strongly enough and can induce a dilute excitonic gas. However, we have found that heterostructures composed of the same TMTC monolayers have higher T_c than vdWH composed of two different TMTC monolayers. Also, T_c of superfluidity in TMTC vdWHs can be manipulated by varying the excitonic density and the number of hBN insulated layers. Finally, we suggest and discuss the possibility of the experimental observation of the angle-dependent superfluidity via Coulomb drag experiments.

Our study demonstrates the angle-dependent superfluidity in TMTC heterostructures, and we hope that it will motivate future experimental and theoretical investigations on excitonic BEC and anisotropic superfluidity in TMTC heterostructures.

ACKNOWLEDGMENTS

The authors are thankful to L. V. Butov for the useful discussion. This work is supported by the U.S. Department of Defense under Grant No. W911NF1810433.

APPENDIX A: BINDING ENERGIES OF INDIRECT EXCITONS IN TMTC vdWH

We calculated the binding energies of indirect excitons in TMTC vdWH using the Coulomb and Rytova-Keldysh potentials. TMTC van der Waals heterostructures that are considered consist from either from the same two TMTC monolayers or two different TMTC monolayers separated by

TABLE I. Binding energies of indirect excitons in TMTC van der Waals heterostructures. Energies are given in meV and electron and hole masses in x and y directions are given in units of the free electron mass.

	Electron ZrSe ₃ ^a	Hole ZrS ₃ ^a	Electron TiS ₃ ^b	Hole ZrS ₃ ^a	Electron TiS ₃ ^b	Hole ZrSe ₃ ^a	Electron ZrS ₃ ^a	Hole ZrS ₃ ^a	Electron ZrS ₃ ^a	Hole ZrSe ₃ ^a	Electron ZrSe ₃ ^a	Hole ZrSe ₃ ^a
m_x	0.16	1.28	1.52	1.28	1.52	2.36	1.3	1.28	1.3	2.36	0.16	2.36
m_y	6.72	0.42	0.4	0.42	0.4	0.89	0.4	0.42	0.4	0.89	6.72	0.89
Potential	V_{RK}	V_C	V_{RK}	V_C	V_{RK}	V_C	V_{RK}	V_C	V_{RK}	V_C	V_{RK}	V_C
1	72.8	105.3	87.7	123.2	87.5	132.8	88.6	121.8	87.7	130.0	73.7	114.5
2	66.5	89.9	78.9	103.6	79.0	110.9	79.6	102.6	79.2	109.0	67.5	97.1
3	61.2	78.7	71.7	89.7	72.0	95.6	72.2	88.9	72.1	94.1	62.2	84.6
4	56.7	70.2	65.7	79.2	66.1	84.2	66.0	78.6	66.2	83.0	57.7	75.1
5	52.7	63.5	60.6	71.1	61.2	75.3	60.9	70.6	61.2	74.3	53.8	67.7
6	49.3	58.0	56.2	64.6	56.9	68.2	56.4	64.1	56.9	67.4	50.3	61.6

^aReference [22].

^bReference [27].

hBN monolayers. Results for the binding energies of indirect excitons in ZrSe₃/ZrS₃, TiS₃/ZrS₃, TiS₃/ZrSe₃, ZrS₃/ZrS₃, ZrS₃/ZrSe₃, ZrSe₃/ZrSe₃ vdWHs are presented in Table I.

APPENDIX B: COUPLING CONSTANT g

The interaction parameters for the exciton-exciton coupling in very dilute systems could be obtained assuming the exciton-exciton repulsion exists only at distances between excitons greater than the distance from the exciton to the classical turning point [54]. Following Ref. [54], one can obtain the coupling constant for the exciton-exciton interaction:

$$g = \int_{R_0}^{\infty} V_{\text{dd}}(R) R dR d\theta, \quad (\text{B1})$$

where $V_{\text{dd}}(R)$ is the dipole-dipole interaction and R_0 corresponds to the distance between two IXs at their classical turning point. R_0 is determined by the conditions that the energy of two excitons cannot exceed the doubled chemical potential μ of the system [54], i.e., $V_{\text{dd}}(R_0) \approx 2\mu$. The last expression is reasonable for a weakly interacting Bose gas of IXs.

To find $V_{\text{dd}}(R)$, consider dipole-dipole interaction as the interactions of positive and negative charges of one dipole with another dipole. Based on well-known screened 2D potential, the Rytova-Keldysh potential V_{RK} [30,31], which is widely used for the description of excitonic complexes in 2D materials [55], a dipole-dipole interaction is obtained in Ref. [56]. The explicit analytical form for the dipole-dipole interaction in 2D configuration space for two excitons has the following form [56]:

$$V_{\text{dd}}(R) = -\frac{\pi k}{2\kappa\rho_0} \left\{ \left[H_{-1}\left(\frac{R}{\rho_0}\right) - Y_{-1}\left(\frac{R}{\rho_0}\right) \right] \frac{\mathbf{d}_1 \cdot \mathbf{d}_2}{\rho_0 R} + \left[H_{-2}\left(\frac{R}{\rho_0}\right) - Y_{-2}\left(\frac{R}{\rho_0}\right) \right] \frac{\mathbf{R} \cdot \mathbf{d}_1 \mathbf{R} \cdot \mathbf{d}_2}{\rho_0^2 R^2} \right\}, \quad (\text{B2})$$

where H_{-1} , H_{-2} and Y_{-1} , Y_{-2} are the Struve functions and Bessel functions of the second kind, respectively. For dipolar excitons formed between two parallel layers separated by

distance D the latter expression becomes

$$V_{\text{dd}}^{\text{RK}}(R) = -\frac{\pi k}{2\kappa\rho_0} \left[H_{-1}\left(\frac{R}{\rho_0}\right) - Y_{-1}\left(\frac{R}{\rho_0}\right) \right] \frac{d^2}{\rho_0 R}, \quad (\text{B3})$$

where $d = eD$ is a dipole moment of the IX. For the Coulomb potential the dipole-dipole interaction of IXs are well known:

$$V_{\text{dd}}^{\text{C}}(\mathbf{R}) = \frac{k d^2}{\kappa R^3}. \quad (\text{B4})$$

After that, it is easy to obtain R_0 for V_C :

$$R_0 = \frac{1}{2\sqrt{\pi n}}. \quad (\text{B5})$$

For the RK potential, we obtain the following equation for R_0 :

$$4\pi n \rho_0^2 y [H_0(y) - Y_0(y)] = -[H_{-1}(y) - Y_{-1}(y)], \quad (\text{B6})$$

where $y = \frac{R_0}{\rho_0}$.

Using the expressions for $V_{\text{dd}}(R)$ [Eqs. (B3) and (B4)] and R_0 [Eqs. (B5) and (B6)], one obtains the exciton-exciton coupling constant g :

$$g = \begin{cases} \frac{\pi^2 k e^2 D^2}{\epsilon_d \rho_0} \left[H_0\left(\frac{R_0}{\rho_0}\right) - Y_0\left(\frac{R_0}{\rho_0}\right) \right] & \text{for } V_{\text{RK}}(x, y), \\ \frac{2\pi k e^2 D^2}{\epsilon_d R_0} = \frac{4\pi k e^2 D^2 \sqrt{\pi n}}{\epsilon_d} & \text{for } V_C(x, y). \end{cases} \quad (\text{B7})$$

APPENDIX C: ANGLE-DEPENDENT NORMAL COMPONENT CONCENTRATION IN AN ANISOTROPIC SYSTEM

The normal density ρ_n for the anisotropic system has tensor form [21] and defined through the component of density flow \mathbf{J} vector as

$$J_i = \frac{n_n^{ij}(T)}{M_j} u_j, \quad (\text{C1})$$

where i and j denote either the x or y components of the vector and $n_n^{(ij)}(T)$ are the tensor elements of normal component concentration. In a superfluid with an anisotropic quasiparticle

energy, the normal-fluid concentration is a diagonal tensor with n_n^{xx} and n_n^{yy} given by [21]

$$n_n^{xx}(T) = \frac{s}{k_B T} \frac{1}{M_x} \frac{1}{(2\pi\hbar)^2} \int d\mathbf{p} \frac{\exp[\varepsilon(p, \phi)/(k_B T)]}{(\exp[\varepsilon(p, \phi)/(k_B T)] - 1)^2} \times \cos^2 \phi, \quad (\text{C2})$$

$$n_n^{yy}(T) = \frac{s}{k_B T} \frac{1}{M_y} \frac{1}{(2\pi\hbar)^2} \int d\mathbf{p} \frac{\exp[\varepsilon(p, \phi)/(k_B T)]}{(\exp[\varepsilon(p, \phi)/(k_B T)] - 1)^2} \times \sin^2 \phi, \quad (\text{C3})$$

$$n_n^{xy}(T) = n_n^{yx}(T) = 0. \quad (\text{C4})$$

Thus, the concentration of the normal component $n_n(\theta, T)$ is

$$n_n(\theta, T) = \sqrt{n_n^{xx}(T)^2 \cos^2 \theta + n_n^{yy}(T)^2 \sin^2 \theta}. \quad (\text{C5})$$

The mean-field critical temperature $T_c(\theta)$ of the phase transition related to the occurrence of superfluidity is determined by the condition

$$n_n(\theta, T_c(\theta)) = n. \quad (\text{C6})$$

APPENDIX D: SOUND MODE OF THE COLLECTIVE EXCITATIONS

In the limit of small momenta p , when $\varepsilon_0(p, \theta) \ll gn$, we expand the spectrum of collective excitations $\varepsilon(p, \theta)$ up to first order with respect to the momentum p and obtain the sound mode of the collective excitations $\varepsilon(p, \theta) = c_s(\theta)p$, where $c_s(\theta)$ is the angle-dependent sound velocity, given by

$$c_s(\theta) = \sqrt{\frac{gn}{M_0(\theta)}}. \quad (\text{D1})$$

The directional anisotropy of the electron and hole masses in TMTC is reflected in the angle-dependent sound velocity. Calculations for $c_s(\theta)$ are performed for different TMTC vdWHs using RK potential and presented in Fig. 2. In Fig. 2 the dashed-dotted and dashed curves present $c_s(\theta)$ in $\text{TiS}_3/\text{ZrS}_3$ and $\text{ZrS}_3/\text{ZrSe}_3$ vdWHs, respectively, while the shaded area presents sound velocities in $\text{ZrS}_3/\text{ZrSe}_3$ and $\text{TiS}_3/\text{ZrSe}_3$. Although in $\text{TiS}_3/\text{TiS}_3$ the sound velocity has a maximum at $\theta = \pi/2$, it weakly depends on the angle due to very close values of μ_x and μ_y . In contrast, $c_s(\theta)$ in $\text{ZrSe}_3/\text{ZrSe}_3$ and $\text{ZrSe}_3/\text{ZrS}_3$ has the same kind qualitative behavior as in phosphorene [18] with minima at $\theta = \pi/2$. We also calculated the sound velocity when electron and hole interact via the Coulomb potential. It should be noted that the sound velocity is greater in the case of Coulomb potential for

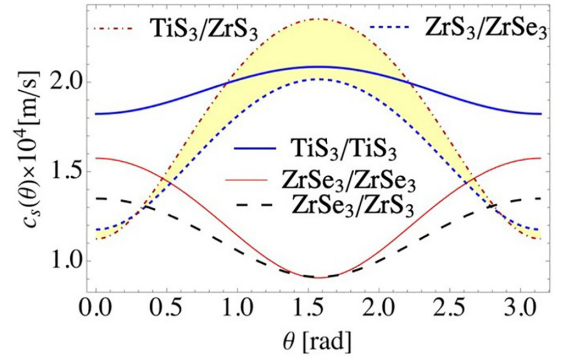


FIG. 2. The angle-dependent sound velocity in different TMTC vdWHs. The interaction between the charged carriers is described by the RK potential. The calculations were performed for the exciton concentration $n = 4 \times 10^{15} \text{ m}^{-2}$ and the number $N_L = 6$ of hBN monolayers placed between two TMTC monolayers.

the interaction between the charge carriers than for the RK potential because the RK potential implies the screening effects, which make the interaction between the carriers weaker. In the case of the soundlike spectrum of collective excitations with the angle-dependent sound velocity $c_s(\theta)$ the integrals (C2) and (C3) can be evaluated analytically using [57] and the results are the following [18]:

$$n_n^{xx}(T) = n_n^{yy}(T) = \frac{2\zeta(3)s(k_B T)^3 \sqrt{M_x M_y}}{\pi(\hbar gn)^2}, \quad (\text{D2})$$

where $\zeta(z)$ is the Riemann zeta function. Therefore, in this case substituting (D2) into (C5) for the concentration of the superfluid component $n_s(T)$ we obtain

$$n_s(T) = n - \frac{2\zeta(3)s(k_B T)^3 \sqrt{M_x M_y}}{\pi(\hbar gn)^2}. \quad (\text{D3})$$

From Eq. (D3) it follows that for the soundlike spectrum of collective excitations, the concentrations of the superfluid components are angle independent. Since at low momenta the soundlike energy spectrum of collective excitations of the indirect exciton in a TMTC heterostructure satisfies the Landau criterion for superfluidity, the superfluidity of IXs in this system is possible. Using Eq. (D2) one can estimate the BKT phase transition temperature from the condition $n_n(T) = n$:

$$T_{\text{BKT}} = \left(\frac{\pi(\hbar g)^2}{2\zeta(3)s\sqrt{M_x M_y}} \right)^{1/3} \frac{n}{k_B}. \quad (\text{D4})$$

This can be considered as an upper bound to the superfluid transition temperature. Thus, for the soundlike spectrum of collective excitations, the T_{BKT} does not depend on an angle.

[1] Y. Lozovik and V. Yudson, On the ground state of the two-dimensional non-ideal bose gas, *Physica A (Amsterdam)* **93**, 493 (1978).

[2] D. W. Snoke, *Dipole Excitons in Coupled Quantum Wells: Toward an Equilibrium Exciton Condensate*, in *Quantum Gases: Finite Temperature and Non-Equilibrium Dynamics*, Vol. 1,

- Cold Atoms Series, edited by N. Proukakis, S. Gardiner, M. Davis, and M. Szymanska (Imperial College Press, London, 2013).
- [3] M. Combescot, R. Combescot, and F. Dubin, Bose-einstein condensation and indirect excitons: A review, *Rep. Prog. Phys.* **80**, 066501 (2017).
- [4] O. L. Berman, R. Y. Kezerashvili, and K. Ziegler, Superfluidity of dipole excitons in the presence of band gaps in two-layer graphene, *Phys. Rev. B* **85**, 035418 (2012).
- [5] Y. E. Lozovik, S. L. Ogarkov, and A. A. Sokolik, Condensation of electron-hole pairs in a two-layer graphene system: Correlation effects, *Phys. Rev. B* **86**, 045429 (2012).
- [6] A. Perali, D. Neilson, and A. R. Hamilton, High-Temperature Superfluidity in Double-Bilayer Graphene, *Phys. Rev. Lett.* **110**, 146803 (2013).
- [7] M. Zarenia, A. Perali, D. Neilson, and F. M. Peeters, Enhancement of electron-hole superfluidity in double few-layer graphene, *Sci. Rep.* **4**, 7319 (2015).
- [8] M. Fogler, L. Butov, and K. Novoselov, High-temperature superfluidity with indirect excitons in van der Waals heterostructures, *Nat. Commun.* **5**, 4555 (2014).
- [9] F.-C. Wu, F. Xue, and A. H. MacDonald, Theory of two-dimensional spatially indirect equilibrium exciton condensates, *Phys. Rev. B* **92**, 165121 (2015).
- [10] M. Zarenia, A. Perali, D. Neilson, and F. M. Peeters, Large gap electron-hole superfluidity and shape resonances in coupled graphene nanoribbons, *Sci. Rep.* **6**, 24860 (2016).
- [11] O. L. Berman and R. Ya. Kezerashvili, High-temperature superfluidity of the two-component Bose gas in a transition metal dichalcogenide bilayer, *Phys. Rev. B* **93**, 245410 (2016).
- [12] O. L. Berman and R. Ya. Kezerashvili, Superfluidity of dipolar excitons in a transition metal dichalcogenide double layer, *Phys. Rev. B* **96**, 094502 (2017).
- [13] S. Conti, A. Perali, F. M. Peeters, and D. Neilson, Multicomponent screening and superfluidity in gapped electron-hole double bilayer graphene with realistic bands, *Phys. Rev. B* **99**, 144517 (2019).
- [14] M. Van der Donck, S. Conti, A. Perali, A. R. Hamilton, B. Partoens, F. M. Peeters, and D. Neilson, Three-dimensional electron-hole superfluidity in a superlattice close to room temperature, *Phys. Rev. B* **102**, 060503(R) (2020).
- [15] S. Conti, S. Saberi-Pouya, A. Perali, M. Virgilio, F. M. Peeters, A. R. Hamilton, G. Scappucci, and D. Neilson, Electron-hole superfluidity in strained Si/Ge type II heterojunctions, *npj Quantum Mater.* **6**, 41 (2021).
- [16] O. L. Berman, G. Gumbs, G. P. Martins, and P. Fekete, Superfluidity of dipolar excitons in a double layer of $\alpha - t_3$ with a mass term, *Nanomaterials* **12**, 1437 (2022).
- [17] C. Ticknor, R. M. Wilson, and J. L. Bohn, Anisotropic Superfluidity in a Dipolar Bose Gas, *Phys. Rev. Lett.* **106**, 065301 (2011).
- [18] O. L. Berman, G. Gumbs, and R. Ya. Kezerashvili, Bose-einstein condensation and superfluidity of dipolar excitons in a phosphorene double layer, *Phys. Rev. B* **96**, 014505 (2017).
- [19] S. Saberi-Pouya, M. Zarenia, A. Perali, T. Vazifeshenas, and F. M. Peeters, High-temperature electron-hole superfluidity with strong anisotropic gaps in double phosphorene monolayers, *Phys. Rev. B* **97**, 174503 (2018).
- [20] Y.-C. Zhang, C.-F. Liu, B. Xu, G. Chen, and W. M. Liu, Two-fluid theory for a superfluid system with anisotropic effective masses, *Phys. Rev. A* **99**, 043622 (2019).
- [21] W. M. Saslow, Normal Fluid Density, Second Sound, and Fourth Sound in an Anisotropic Superfluid, *Phys. Rev. Lett.* **31**, 870 (1973).
- [22] Y. Jin, X. Li, and J. Yang, Single layer of MX_3 ($M = \text{Ti, Zr}$; $X = \text{S, Se, Te}$): A new platform for nano-electronics and optics, *Phys. Chem. Chem. Phys.* **17**, 18665 (2015).
- [23] M. Li, J. Dai, and X. C. Zeng, Tuning the electronic properties of transition-metal trichalcogenides via tensile strain, *Nanoscale* **7**, 15385 (2015).
- [24] L. Britnell, R. V. Gorbachev, R. Jalil, B. D. Belle, F. Schedin, M. I. Katsnelson, L. Eaves, S. V. Morozov, A. S. Mayorov, N. M. R. Peres, A. H. Castro Neto, J. Leist, A. K. Geim, L. A. Ponomarenko, and K. S. Novoselov, Electron tunneling through ultrathin boron nitride crystalline barriers, *Nano Lett.* **12**, 1707 (2012).
- [25] M. Combescot, O. Betbeder-Matibet, and F. Dubin, The many-body physics of composite bosons, *Phys. Rep.* **463**, 215 (2008).
- [26] Y. Saeed, A. Kachmar, and M. A. Carignano, First-principles study of the transport properties in bulk and monolayer MX_3 ($M = \text{Ti, Zr, Hf}$ and $X = \text{S, Se}$) compounds, *J. Phys. Chem. C* **121**, 1399 (2017).
- [27] M. Van der Donck and F. M. Peeters, Excitonic complexes in anisotropic atomically thin two-dimensional materials: Black phosphorus and TiS_3 , *Phys. Rev. B* **98**, 235401 (2018).
- [28] C. Wang, C. Zheng, and G. Gao, Bulk and monolayer ZrS_3 as promising anisotropic thermoelectric materials: A comparative study, *J. Phys. Chem. C* **124**, 6536 (2020).
- [29] N. Tripathi, V. Pavelyev, P. Sharma, S. Kumar, A. Rymzhina, and P. Mishra, Review of titanium trisulfide (TiS_3): A novel material for next generation electronic and optical devices, *Mater. Sci. Semicond. Process.* **127**, 105699 (2021).
- [30] N. S. Rytova, The screened potential of a point charge in a thin film, *Proc. MSU Phys., Astron.* **3**, 30 (1967).
- [31] L. V. Keldysh, Coulomb interaction in thin semiconductor and semimetal films, *Pis'ma Zh. Eksp. Teor. Fiz.* **29**, 716 (1979)[*JETP Lett* **29**, 658 (1979)].
- [32] P. Cudazzo, I. V. Tokatly, and A. Rubio, Dielectric screening in two-dimensional insulators: Implications for excitonic and impurity states in graphene, *Phys. Rev. B* **84**, 085406 (2011).
- [33] T. C. Berkelbach, M. S. Hybertsen, and D. R. Reichman, Theory of neutral and charged excitons in monolayer transition metal dichalcogenides, *Phys. Rev. B* **88**, 045318 (2013).
- [34] S. A. Moskalenko and D. W. Snoke, *Bose-Einstein Condensation of Excitons and Biexcitons and Coherent Nonlinear Optics with Excitons* (Cambridge University Press, New York, 2000).
- [35] E. M. Lifshitz and L. P. Pitaevskii, *Statistical Physics, Part 2* (Pergamon, Oxford, 1980).
- [36] L. P. Pitaevskii and S. Stringari, *Bose-Einstein Condensation and Superfluidity* (Oxford University Press, Oxford, 2016).
- [37] A. Abrikosov, L. Gorkov, and I. Dzyaloshinskii, *Methods of Quantum Field Theory in Statistical Physics* (Prentice-Hall, Englewood Cliffs, NJ, 1963).
- [38] N. N. Bogolyubov, On the theory of superfluidity, *J. Phys. (USSR)* **11**, 23 (1947).
- [39] L. P. Pitaevskii and S. Stringari, *Bose-Einstein Condensation and Superfluidity* (Oxford University Press, Oxford, 2003).

- [40] J. Bardeen, Two-fluid model of superconductivity, *Phys. Rev. Lett.* **1**, 399 (1958).
- [41] L. H. Fowler-Gerace, Z. Zhou, E. A. Szwed, and L. V. Butov, Long-range quantum transport of indirect excitons in van der Waals heterostructure, [arXiv:2204.09760](https://arxiv.org/abs/2204.09760).
- [42] A. Surrente, A. A. Mitioglu, K. Galkowski, L. Klopotoski, W. Tabis, B. Vignolle, D. K. Maude, and P. Plochocka, Onset of exciton-exciton annihilation in single-layer black phosphorus, *Phys. Rev. B* **94**, 075425 (2016).
- [43] D. J. Choksy, E. A. Szwed, L. V. Butov, K. W. Baldwin, and L. N. Pfeiffer, Fermi edge singularity in neutral electron-hole system, [arXiv:2209.06026](https://arxiv.org/abs/2209.06026).
- [44] J. L. Hodeau, M. Marezio, C. Roucau, R. Ayroles, A. Meerschaut, J. Rouxel, and P. Monceau, Charge-density waves in NbSe₃ at 145K: Crystal structures, X-ray and electron diffraction studies, *J. Phys. C: Solid State Phys.* **11**, 4117 (1978).
- [45] A. Ait-Ouali and S. Jandl, Two-dimensional indirect excitons in the layer-type trichalcogenide ZrS₃, *Phys. Rev. B* **49**, 1813 (1994).
- [46] A. Pant, E. Torun, B. Chen, S. Bhat, X. Fan, K. Wu, D. P. Wright, F. M. Peeters, E. Soignard, H. Sahin, and S. Tongay, Strong dichroic emission in the pseudo one dimensional material ZrS₃, *Nanoscale* **8**, 16259 (2016).
- [47] T. J. Wieting, A. Grisel, F. Lévy, and P. Schmid, Quasi-one-dimensional conductors I, *Lect. Notes Phys.* **95**, 354 (1979).
- [48] A. Grisel, F. Lévy, and T. Wieting, Optical-phonon anisotropies in crystalline IVB trichalcogenides, *Physica B+C (Amsterdam)* **99**, 365 (1980).
- [49] A. S. Rodin, A. Carvalho, and A. H. Castro Neto, Excitons in anisotropic two-dimensional semiconducting crystals, *Phys. Rev. B* **90**, 075429 (2014).
- [50] E. Torun, H. Sahin, A. Chaves, L. Wirtz, and F. M. Peeters, Ab initio and semiempirical modeling of excitons and trions in monolayer TiS₃, *Phys. Rev. B* **98**, 075419 (2018).
- [51] R. Y. Kezerashvili and A. Spiridonova, Anisotropic magnetoexcitons in two-dimensional transition metal trichalcogenide semiconductors, *Phys. Rev. Res.* **4**, 033016 (2022).
- [52] B. N. Narozhny and A. Levchenko, Coulomb drag, *Rev. Mod. Phys.* **88**, 025003 (2016).
- [53] D. Nandi, A. D. K. Finck, J. P. Eisenstein, L. N. Pfeiffer, and K. W. West, Exciton condensation and perfect Coulomb drag, *Nature (London)* **488**, 481 (2012).
- [54] O. L. Berman, R. Ya. Kezerashvili, G. V. Kolmakov, and Y. E. Lozovik, Turbulence in a Bose-Einstein condensate of dipolar excitons in coupled quantum wells, *Phys. Rev. B* **86**, 045108 (2012).
- [55] R. Y. Kezerashvili, Few-body systems in condensed matter physics, *Few-Body Syst.* **60**, 52 (2019).
- [56] R. Y. Kezerashvili and V. Ya. Kezerashvili, Charge-dipole and dipole-dipole interactions in two-dimensional materials, *Phys. Rev. B* **105**, 205416 (2022).
- [57] I. S. Gradshteyn and I. M. Ryzhik, *Tables of Integrals, Series, and Products* (Academic, New York, 1965).